JOURNAL OF MATERIALS SCIENCE 18 (1983) 930–942

The metallography and deformation of the aligned Cd–Zn eutectic

Part 1 *Compression*

C. J. DAVIDSON, I. O. SMITH
Department of Mining and Metallurgical Engineering, University of Queensland, St. Lucia, Qld. 4067, Australia

The influence of interlamellar spacing (λ) and heat-treatment on the compressive deformation of unidirectionally solidified Cd–Zn eutectic alloys has been investigated by precision strain measurements during compressive loading and by optical and transmission electron metallography. The flow stress at a measured plastic strain of 1×10^{-6} increased markedly with decreasing λ. The strain hardening rate was linear between plastic strains of 10^{-5} and about 5×10^{-3} and was independent of λ. Basal glide was found to be the predominant deformation process during the linear strain hardening and it led to kink band formation at plastics strains of approximately 6×10^{-3}. Probable causes of the dependence of deformation mechanics on λ are examined.

1. Introduction

The influence of interlamellar spacing on the compressive deformation of the Cd–Zn eutectic was first demonstrated by Shaw [1] who observed that the material exhibited a sharp upper yield point which occurred at a stress proportional to $\lambda^{-0.5}$. The model which Shaw proposed to explain the results was a variation of the Hall–Petch model of grain-size dependence. In the case of the eutectic alloy, dislocations were assumed to pile up against the interphase boundary prior to observable yield and, at the yield point, to be forced through the interface onto parallel glide planes in an adjacent lamella. The inverse square root dependence of stress on λ then followed from an argument similar to the one relating yield stress to grain size in polycrystalline materials. The substantial drop in stress following yield was thought to represent either the diminution of the ability of the boundary to resist further slip or rapid multiplication of dislocation sources in a localized area.

Sahoo *et al.* [2] have also studied the compressive deformation of this eutectic alloy and its relationship to λ. In contrast to Shaw, they did not observe a yield point. However, they reported ultimate compressive stress (UCS) values which, for any given growth rate, were slightly lower than the yield stress values of Shaw. Evidently there is a discrepancy between the interpretations of the deformation characteristics which need to be resolved.

The functional dependence of 0.2% proof stress on growth rate was investigated by Sahoo *et al.* [2] who observed a similar relationship to that found by Shaw for the yield stress dependence on growth rate. Sahoo *et al.* and Shaw differ in their explanations of the findings. The former noted that the orientation of both phases is one where the basal plane is nearly parallel to the compression axis, and thus the resolved stress for basal glide would be very low. From this they concluded that $\{11\bar{2}2\}\langle 11\bar{2}3\rangle$ pyramidal slip was responsible for the observed deformation structure. They did not accept Shaw's contention that the interphase boundary would provide a significant obstacle to slip and, instead, proposed that the large numbers of grown-in crystal defects associated with rotation of the crystal structure at solidification cell boundaries were responsible for the strenghening. In later experimental work it was

0022–2461/83/030930–13$04.06/0

reported [3] that the crystal orientation did not change near the cell boundaries and consequently there was no significant variation in the dislocation density.

Thus, the controlling deformation processes are still not clear and it was decided in this study to combine sensitive mechanical tests with optical and electron metallography to try to obtain a more complete picture of the deformation processes.

2. Experimental details

An alloy of eutectic composition (17.4 wt % Zn) was prepared from materials of 99.999 % purity by melting and casting under argon and swaging to 6 mm diameter. A section of this rod was then placed in a graphite mould and drawn vertically downwards through an induction furnace at rates between 0.5 and 300 μm sec^{-1}. The temperature gradient was approximately 4 K mm^{-1}.

Cylinders slightly greater than 5 mm in diameter were machined from the unidirectionally solidified ingot with the axis parallel to the growth direction and electropolished to 5 mm diameter. These were cut into 11 mm lengths and fixed in a steel jig. The ends were then metallographically polished to be flat and parallel, with a final specimen length of 10 mm.

An apparatus similar to that used by Meakin [4] for micro-strain testing was employed to provide the high sensitivity strain detection during the compression testing. The strain was taken from the average output of two diametrically opposed l.v.d.t.* strain transducers. A nominal strain rate of 5×10^{-4} sec^{-1} was used for all tests except those investigating strain-rate sensitivity.

Load and elongation were recorded on an x–y recorder with 10 step zero suppression on each axis. Data was read from the charts with a digitizer and analysed directly by a computer program to produce true stress, true strain (assuming homogeneous deformation) and plastic strain. A correction was made to the strain data from compression tests by subtracting the theoretical uniform elastic deformation of the anvils between the l.v.d.t. points of attachment. However the consistency with which the measured elastic modulus was lower in compression than in tension tests [5] indicated that significant indentation of the anvils was taking place. It was not possible to apply a correction for this.

Most tests were carried out on the material in the as-solidifed state, although several specimens were solution-treated at 513 K for 15 min and then water quenched. The time at elevated temperature was just sufficient to avoid spheroidization of the lamellar structure of the most finely spaced alloy.

Thin foils of longitudinal and transverse sections were prepared for transmission electron microscopy by jet machining in a solution of 10 % H_3PO_4 in water followed by final electropolishing in 10 % $HClO_4$ in ethanol at 10 V at a temperature of 220 K. Analysis of diffraction patterns obtained was aided by a computer program based on that of Booth *et al.* [6]. Multiple solutions were obtained with many diffraction patterns, particularly those of lower order, and these had to be resolved by tilting slightly to provide a second pattern and a second set of solutions.

Analysis of crystallographic orientation was carried out by Kikuchi pattern examination and by X-ray texture analysis. To enable the sharp texture to be accurately plotted the automatic spiral scanning pattern was disabled and the peaks scanned in a much closer, manually selected pattern.

3. Results

3.1. Solidification

Microstructures seen in transverse and longitudinal sections were similar to those reported by other workers, e.g. Sahoo *et al.* [2]. None of the ingots was strictly monocrystalline; the structure varied from grains about 3 mm in diameter at a growth rate of 0.5 μm sec^{-1} to cells approximately 0.2 to 0.3 mm wide at a growth rate of 300 μm sec^{-1}. Adjacent cells showed only small variations in orientation and the grain/cell size changed little among growth rates of 12 μm sec^{-1} and faster. Although alloys with these moderate growth rates appeared cellular at low magnifications, curvature of the solid–liquid interface (i.e. misalignment of the lamellae in cell boundaries) was not evident in longitudinal sections until samples with solidification rates of 120 μm sec^{-1} or greater were examined. There was no observed coarsening during the cooling following solidification or during the time spent near room temperature during specimen preparation. The measured dependence of interlamellar spacing on solidification rate is included in Table I.

*l.v.d.t.–linear variable differential transformer.

TABLE I Results of compression tests on Cd–Zn eutectic alloys

Alloy	Growth rate ($\mu m\ sec^{-1}$)	λ (μm)	E ($GN\ m^{-2}$)	Stress ($MN\ m^{-2}$)					$\epsilon_{plastic}$ at σ_{max} ($\times 10^{-3}$)	Remarks
				yield	10^{-5}	10^{-4}	10^{-3}	σ_{max}		
A1	0.5	5.1	70.2	33	47.9	70.2	116.6	146	16.7	Severe banding
A2			–	–	–	–	–	141		Moderate banding
B1	2.0	2.7	86.1	–	–	79.7	117.1	170	4.4	Severe banding
B2			70.5	43	52.9	81.8	123.1	> 150	> 8.5	Unloaded prior to σ_{max}
B3			71.5	49	59.8	72.8	113.4	164	4.8	Moderate banding
B4			72	–	55	68.1	100.8	155.8	6.3?	Unload/reload test
B5			77.8	94.7	148.9	209.3	260	281	3.4	Quenched; unload/reload test
C1	12	1.5	86.7	59	86.4	96.8	120.2	> 229	> 7.7	Unload prior to σ_{max}
C2			76.5	72	83.8	98.1	123.1	220	7.1	
C3			74.7	132.4	153.9	168.5	204.1	303	6.4	Quenched
D1	30	0.72	91	38	60.9	105.3	138.4	246	7.5	
D2			81.3	62	109.2	123	147.4	251	6.2	
D3			70.4	68.7	82.4	115.8	147.9	264.6	6.5	Crosshead speed: 0.01 mm sec^{-1}
D4			77.9	–	126	156	283	284	6.5	Crosshead speed: 0.15 mm sec^{-1}
E1	120	0.4	79.8	78	124.9	158	189	325	6.6	
E2			76.4	79	107.3	149.6	185.2	309	6.6	
E3			70.4	90.1	118.1	142	181	322.3	6.6	
E4			75.4	99.3	124.9	148.7	182.7	–		Unloaded prior to σ_{max}
E5			78.3	124.5	139.8	155	189.6	300.8	7.0?	Unload/reload test
F1	300	0.35	82.2	110	125.4	187.1	224.7	357	6.2	
F2			77.3	112	142.7	182.6	218.1	366	7.1	
F3			72.4	169	181.8	200.2	234.7	392	9.7	Quenched

Both X-ray texture and electron diffraction analyses revealed that the orientation relationships were the same as those previously published [1, 7], namely:

$$(0001)_{Cd} \parallel (0001)_{Zn} \parallel \text{lamellar interface} \pm 1^\circ$$

$$[11\bar{2}0]_{Cd} \parallel [11\bar{2}0]_{Zn} \parallel \text{growth direction} \pm 5^\circ$$

Analysis of the Kikuchi patterns from transmission electron microscopy showed that the above relationship between the two phases was followed more precisely than is usual for eutectic alloys, with orientation variations of less than 0.5 degrees between adjacent lamellae.

X-ray pole figures obtained from specimens solidified at several different rates are plotted in Fig. 1. Beyond 2 cm of the start of the ingot, the ingot axis remained within 5 degrees of $[11\bar{2}0]$. One trend apparent in Fig. 1 is that, as growth rate was increased, the crystallographic orientation normal to the growth direction became more random.

3.2. Mechanical testing

Representative stress–strain curves of the compression tests are shown in Fig. 2. Characteristic features are a relatively clear transition to plastic deformation followed by an approximately linear strain-hardening stage until, at about 0.01 strain, there is a maximum stress, σ_{max}. All alloys except those with the coarsest interlamellar spacing exhibited the linear strain hardening. Fig. 3 shows that the plastic strain-hardening rate of these specimens in the linear region was independent of interlamellar spacing. When the maximum stress was attained the specimen entered a state of plastic instability, there being a very rapid drop in load and concurrent rapid decrease in specimen length. The smaller the interlamellar spacing, the more pronounced was the effect. Confirmation of the unstable nature of the specimen was provided by performing a series of unload/reload tests on selected specimens. The result of one such test is illustrated in Fig. 4. Unloading from the linear strain-hardening region showed the usual response of single phase materials: elastic deformation only, followed by resumption of plastic flow upon reloading to the previous stress level (there was usually a small reloading yield point but the cause of this was not investigated). However the eutectic alloy differed considerably from single phase materials if unloading commenced

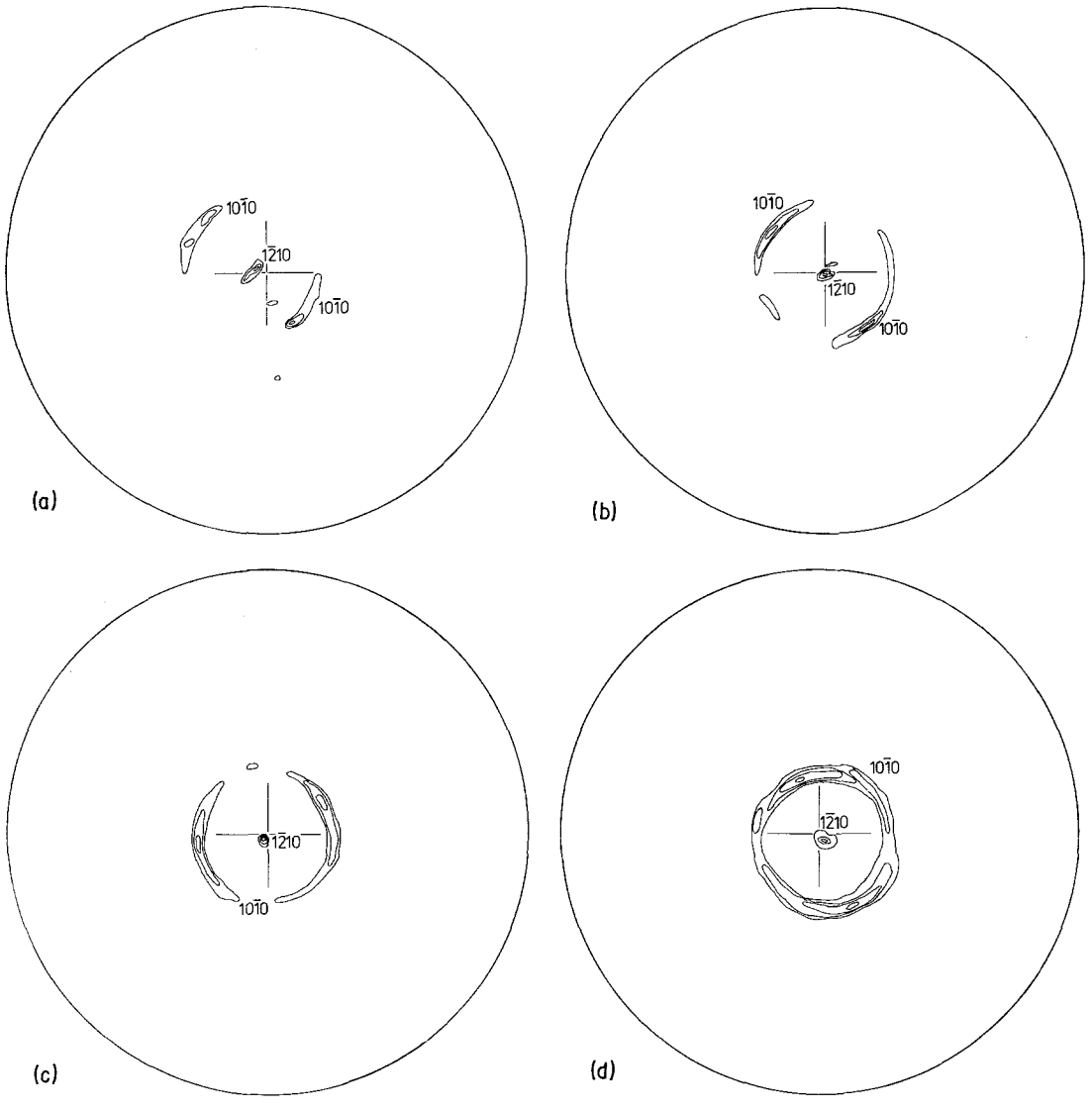

Figure 1 Pole figures from the centre of ingots of directionally solidified Cd–Zn eutectic alloy showing the variation of texture with growth rate (transverse section) (a) solidification rate 2 μm sec^{-1}, (b) solidification rate 12 μm sec^{-1}, (c) solidification rate 120 μm sec^{-1}, and (d) solidification rate 300 μm sec^{-1}.

at a point near the maximum stress. At this stage considerable forward plastic flow took place while the crosshead was reversing.

Table I gives the information obtained from the compression tests. The yield stress is defined as the flow stress at a plastic strain of 10^{-6}. The yield, flow and maximum stresses are plotted in Fig. 5 as a function of $\lambda^{-0.5}$. While σ_{max} could be said to be linearly dependent on $\lambda^{-0.5}$ there is no evidence for a similar relationship with any of the other stress parameters.

The influence of strain-rate on compressive deformation was investigated at growth rate D at strain-rates between 5×10^{-4} and 1.5×10^{-2} sec^{-1}. The value of σ_{max} was found to increase by about 10% for a tenfold increase in strain-rate.

Strength was improved somewhat by a solution treatment followed by a water quench. This increase was greater for alloys with larger values of λ, although in all cases quenching produced a substantial increase in flow stress at plastic strains beyond σ_{max}.

3.3. Metallography

Fig. 6 shows photomacrographs of typical compression samples after about 10% deformation.

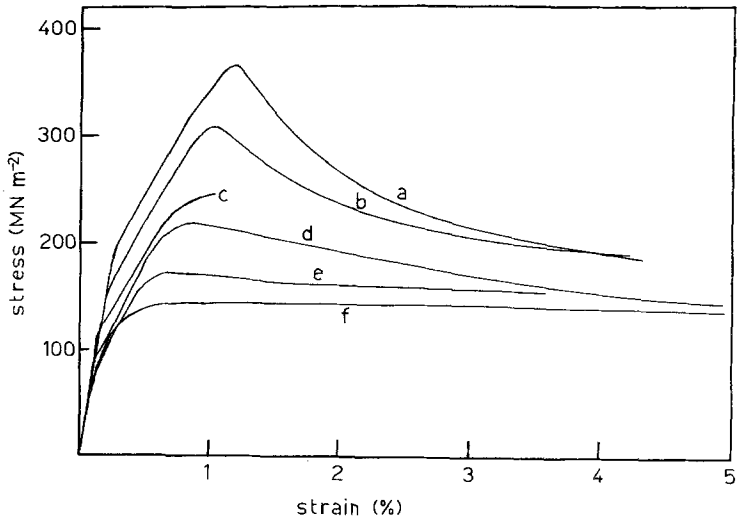

Figure 2 Compressive stress–strain curves for a typical sample from each growth rate. Specimen details are given in Table I. The strain at which each curve stops marks the point at which that specimen was unloaded for metallographic examination. Curve a, specimen F2; curve b, specimen E2; curve c, specimen D1; curve d, specimen C2; curve e, specimen B3; and curve f, specimen A1.

Each pair shows the surface appearance and a polished longitudinal section of the same sample. As can be seen from the Fig. 6, the deformation bands had a relatively homogeneous distribution at large interlamellar spacings but became very localized at the finest spacings. Although deformation tended to be concentrated in a particular area in the more coarsely spaced samples, there was evidence of some deformation throughout the sample. In contrast to this, the finer specimens showed very little deformation outside the narrow deformation band. These observations conform with those of Shaw who reported that specimens with larger values of λ deformed with bulges on the surface and those with λ of 2.5 μm and less deformed with steps on the surface. It is apparent from Fig. 6 that in these tests the transition was not quite as abrupt as was implied by Shaw; the area of localized deformation gradually became narrower as λ decreased from 2.7 to 0.72 μm; The typical deformation structure can be more closely examined in Fig. 7. Basically, the deformation microstructure is similar to those reported previously [1, 2] with an increasing tendency to spheroidize during deformation as λ decreases. However, close examination casts some doubt on the previous interpretation of the deformation microstructure. It was suggested by Shaw and subsequently accepted by Soutiere and Kerr [8] and by Sahoo *et al.* [2] that there were two distinct types of deformation:

1. slip lines, or smoothly bent lamellae; and
2. kink bands, or sharply bent lamellae.

Extensive optical microscopy in this study has failed to distinguish clearly between these two types. As can be seen in Fig. 7 a sharp "kink band" may gradually lose its sharp boundary and became a "slip line". The major impression was that both types represent the same deformation structure at different stages of development.

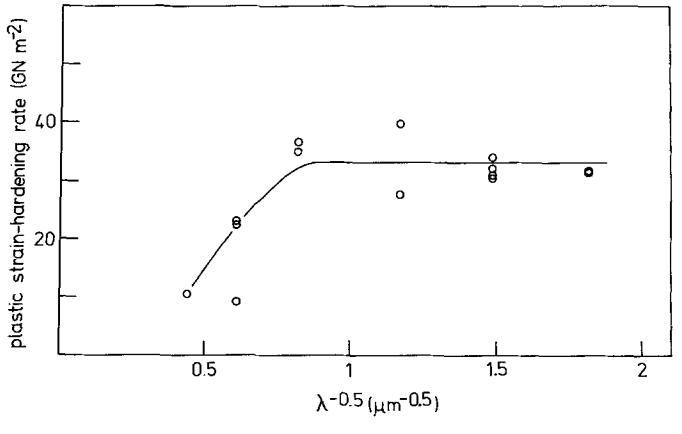

Figure 3 Plot illustrating the influence of λ on plastic strain-hardening rate at a plastic strain of 2×10^{-3}.

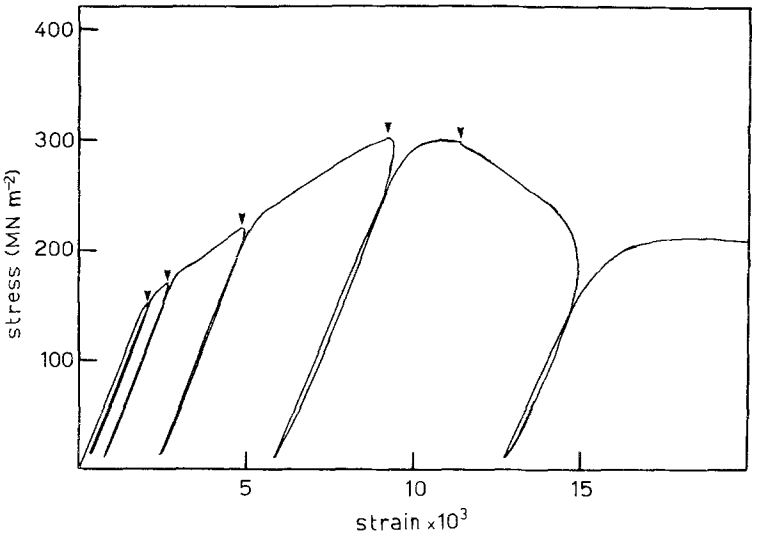

Figure 4 Compressive stress–strain behaviour of specimen E5 during unloading and reloading. Arrows mark points of cross-head reversal.

An outline of the sequence of events during compression was gained by unloading specimens after various amounts of deformation. Samples unloaded from about 70% of σ_{max} (prior to reaching it) did not show any signs of plastic deformation under examination by optical microscopy. However deformation bands were observed as soon as the specimen reached σ_{max}. The formation of the first kinks led to rapid softening and continued forward deformation during unloading. Specimen E3 was unloaded after compression to a strain of 3×10^{-5} beyond σ_{max} and it was observed that the deformation band had completely lost its lamellar microstructure. Thirty per cent of the total forward plastic strain of the specimen occurred during unloading and it was during this short period that the initial deformation band would have extended. Spheroidization of the lamellar microstructure within the band would have occurred during unloading and also at room temperature before sectioning and polishing took place.

Examination by electron microscopy of specimens in the as-grown state showed a very low density of dislocations. A typical electron micrograph of a deformation band is shown in Fig. 8. The common characteristics are a high-angle grain boundary which sharpely delimits the deformation band and other low-angle boundaries usually extending across individual lamellae. Orientation changes in the Cd-phase across high-angle boundaries were matched precisely by changes in zinc orientation. That is, the original interphase orientation relationships were maintained within deformation bands.

Testing of quenched eutectic alloys showed not only a higher strength but also a significantly different microstructure. Fig. 9 shows macro- and micrographs of a quenched specimen with $\lambda = 1.5\,\mu m$. The bulges on the surface appear much finer than for the as-grown alloy and the variation with λ is minimal, in contrast to the large differences evident in Fig. 6. Optical microscopy also revealed that the deformation bands were finer and much more numerous in the quenched alloys than in the untreated ones. Moreover deformation induced coarsening was largely suppressed, even in the most finely spaced alloys.

The electron microstructure in a quenched and deformed specimen can be seen in Fig. 9c. The major difference noted between quenched and as-grown materials after compression is the prevalence of numerous low-angle boundaries in the former. In these dislocation arrays the individual dislocations are easily resolved, in contrast to the low-angle boundaries of, for example, Fig. 8. Such low density arrays were not a common feature of those specimens which received no heat-treatment, while on the other hand they were predominant in quenched alloys. No direct cause of the differences between as-grown and quenched alloys was seen.

4. Discussion

4.1. Deformation behaviour

Differences exist within the literature as to the features of a normal compressive stress-strain curve. Shaw [1] refers to a yield point, which was not observed either by Sahoo *et al.* [2] or in this

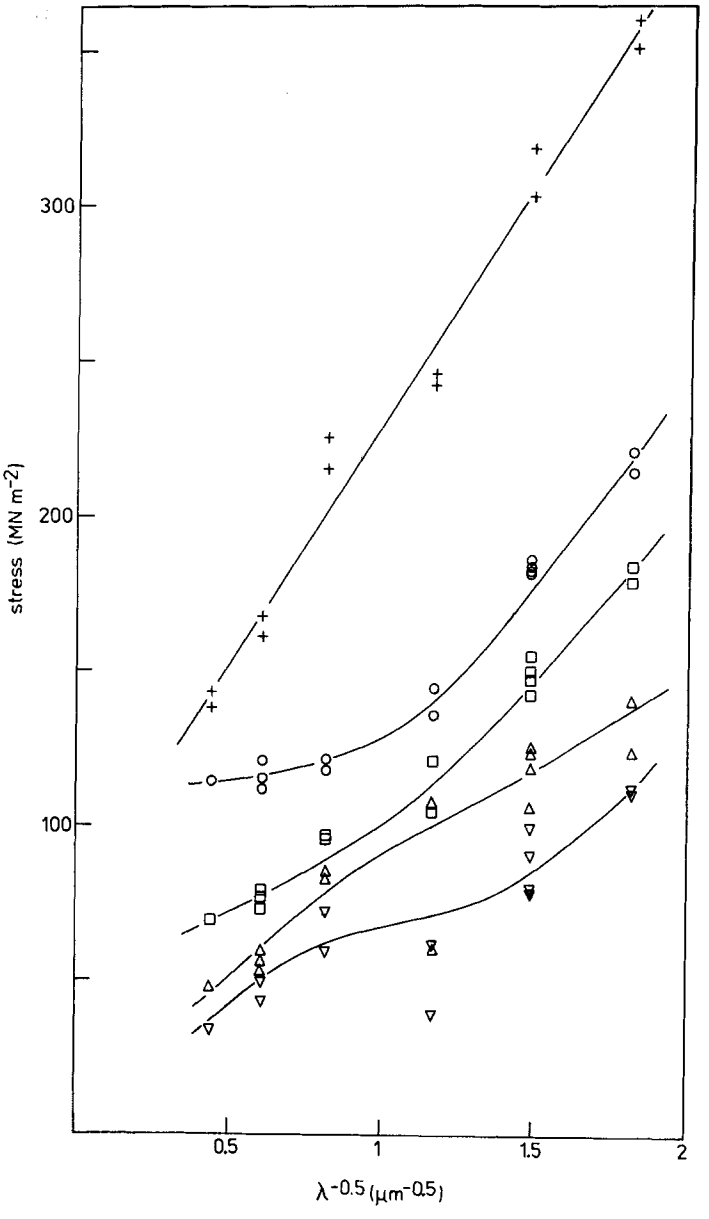

Figure 5 Compressive yield, flow and maximum stresses against $\lambda^{-0.5}$ for all specimens. ▽ yield; △ 10^{-5}; □ 10^{-4}; ○ 10^{-3}; + σ_{max}.

work. However close examination reveals that, at comparable λ, the values of σ_{max} measured in this study are very close to those designated by Shaw as the upper yield stress or by Sahoo *et al.* as the UCS. Looking at the stress–strain curves in Fig. 2 it becomes apparent that the interpretation of Sahoo *et al.*, rather than that of Shaw, is correct and the difference would most likely have arisen due to inadequate strain resolution in Shaw's testing method.

Orowan [9] was the first to describe kink bands observed during compression of single crystal cadmium in a similar orientation of that of the Cd–Zn eutectic. Hess and Barrett [10] noted that, for kink banding to occur in zinc, the compression axis was required to be a few degrees from parallel to (0001). They proposed a model where plastic deformation occurs by normal basal glide and low-angle tilt boundaries that are formed grow into high-angle kink boundaries. Kink boundaries were often observed to be sharp in some places, gradually becoming diffuse and rounded.

The deformation bands seen in the Cd–Zn eutectic fit well to the description and requirements of Hess and Barrett for kink bands and substantial support for this model is provided by transmission electron microscope observations.

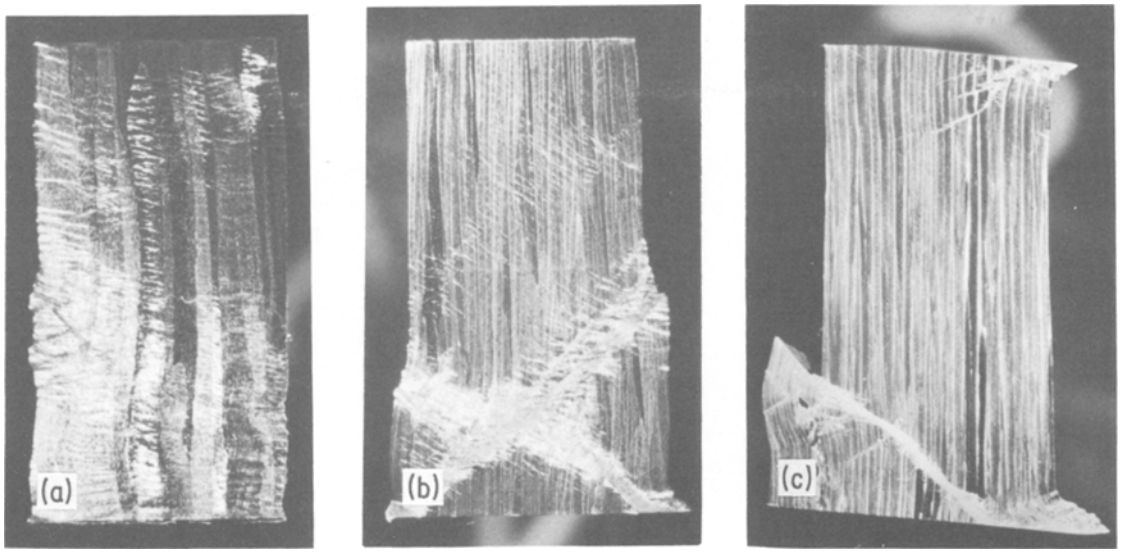

Figure 6 Photomacrographs of longitudinal sections of specimens deformed approximately 10% in compression. (a) B3, (b) C2 and (c) F2.

The orientation changes of more than 10 kink boundaries were examined in detail by transmission electron microscopy to check the prediction of the Hess and Barrett model that they were formed by rotation about a direction in the basal phase normal to the Burger's vector (i.e. about $[10\bar{1}0]$). Using Kikuchi lines to accurately determine the orientation of each section, pairs of stereographic projections could be compared. In only a couple of cases did this show a possible rotation axis very close to $[10\bar{1}0]$. While this indicates that in most cases a single glide system could not be responsible for the kink structure, Hess and Barrett noted that duplex glide would produce irrational rotation axes. Re-examination of the crystallography showed that it was always possible to transpose from one orientation to the other by successive rotations about two $\langle 10\bar{1}0\rangle$ directions. This provides strong evidence for a deformation process similar to that described by Hess and Barrett.

Fig. 10 shows the dislocation structure in what has been identified as the tip of a kink band. The high density of dislocations in the unkinked region were most likely present to accommodate the large internal strains caused by the kink. Of those dislocations examined more closely, all proved to have $\langle 11\bar{2}0\rangle$ type Burger's vectors. Most were arranged in low-angle boundaries.

Further confirmation of the kink band model was obtained by examining specimens unloaded before the kinking stress was reached. Many lamellae did not seem to contain any dislocations but, in those that did, the most common arrangement was that shown in Fig. 11. They have $\langle 11\bar{2}0\rangle$ type Burger's vectors and appear to be queuing on the basal plane; behaviour consistent with the kink band model. The possibility that these dislocations were formed during foil handling is largely discounted as they were observed consistently in these specimens but not all in the as-grown material.

4.2. Interlamellar spacing dependence

Shaw's explanation for the strength dependence on λ was based on a model of dislocation pile-up against the interphase boundary. Sahoo *et al.* [2] were more specific when they assumed that the dominant glide system would have to be $\{11\bar{2}2\}\ \langle 11\bar{2}3\rangle$ to explain the observed "slip bands". Burger's vector analysis did not reveal any of the $\langle 11\bar{2}3\rangle$ type, all were $\langle 11\bar{2}0\rangle$, and evidence for the operative slip plane favours basal glide rather than pyramidal. Thus it appears that dislocation motion is parallel to the lamellar interface which therefore cannot be a barrier to slip.

Results derived from the mechanical and metallographic testing of the Cd–Zn eutectic alloy invite conflicting interpretations of the nature of its compressive deformation. The metallography clearly points to basal glide predominating at all

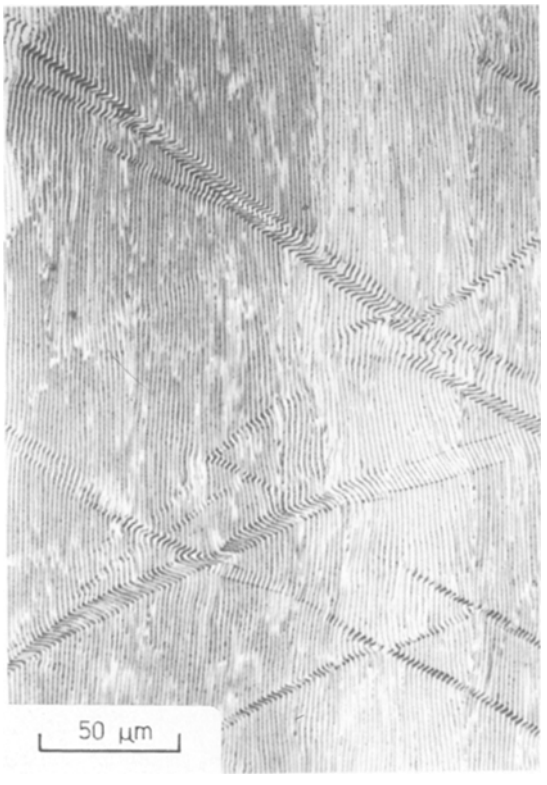

Figure 7 Typical optical micrograph of Cd–Zn eutectic alloy deformed in compression showing gradual shift from sharp to smooth deformation bands (specimen C1, compression axis vertical).

stages of plastic deformation and to the formation of kink bands from these basal dislocations. On the other hand it may be inferred from the strong dependence of flow and kinking stresses on λ that the proximity of the interphase boundary plays an important part in regulating plastic flow. It is difficult to envisage how the interface could so effectively control shear on planes to which it is parallel. Several possible sources of such control must be examined. These include those which are significant in any composite alloy, such as solution strengthening, residual stresses and constraint and they will be examined in detail below.

Examination of Table I shows that, with the exception of the most coarsely spaced alloys, the plastic strain at σ_{max} was about 7×10^{-3} and was independent of λ. Here the implication is that the axial rate from kink formation exceeded the crosshead displacement rate after a fixed amount of basal glide, independent of λ (The variations at large λ are possibly caused by the banded structure developed during solidification). Similarly the strain hardening rate prior to kinking shows relatively little dependence on λ. Thus it is only in the microstrain region that a strong influence of λ is apparent and stress differentials developed at that stage maintained through subsequent stages of deformation.

Possible factors involved in the influence of λ on stress in the microstrain region will now be examined.

4.2.1. Solution strengthening

Solid solution strengthening would undoubtedly be responsible for raising the strength of the eutectic material above either of the pure components. However variations in solid solution concentration levels with growth rate is unlikely to be a significant factor in the λ dependence on strength since alloys which had been subjected to a solution heat-treatment show increased strength with

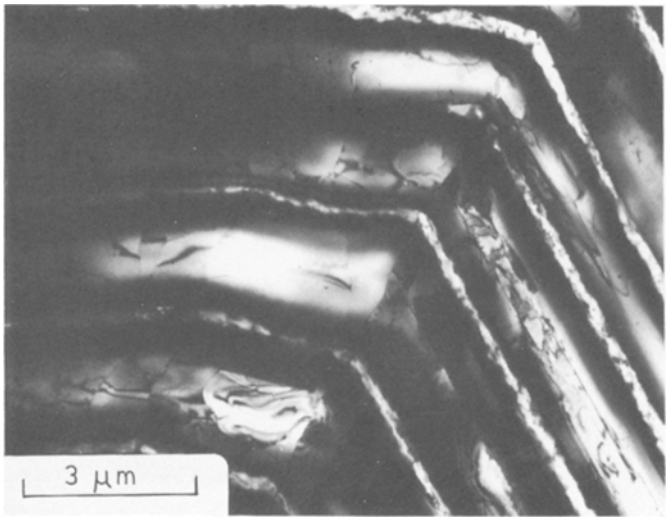

Figure 8 Transmission electron micrograph of high-angle boundary in deformation band. Also illustrated are the low-angle boundaries within the band. (Specimen A1; longitudinal section).

decreased λ. It would be expected that, immediately after quenching, solution levels would be independent of λ and that any reduction due to room temperature annealing would be greatest in the more finely spaced alloys through expitaxial precipitation on the adjacent lamellae. However alloys with smaller λ are still stronger.

4.2.2. Residual stress

The next factor to be considered is the residual stress state induced during cooling from the eutectic melting temperature. The method of Laszlo [11] was employed to estimate the maximum residual stress in each phase. Using single crystal data for elastic constants [12] and thermal expansion coefficients [13] gave the following results:

$$\sigma_{Zn} = 158\,\mathrm{NM\,m^{-2}} \text{ in compression}$$

$$\sigma_{Cd} = 40\,\mathrm{MN\,m^{-2}} \text{ in tension}$$

Estimation of the residual stresses by com-

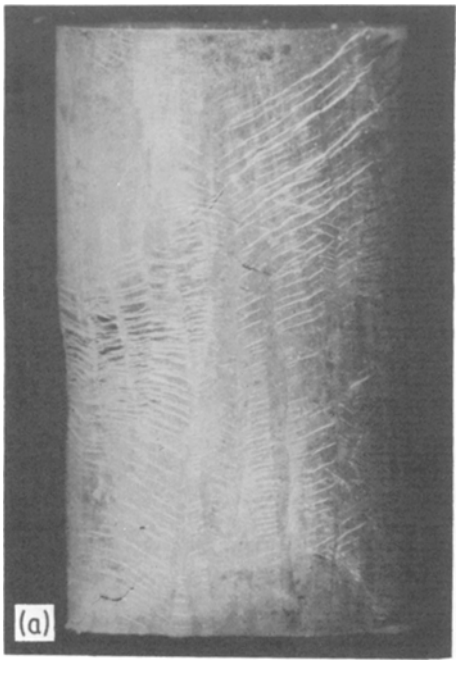

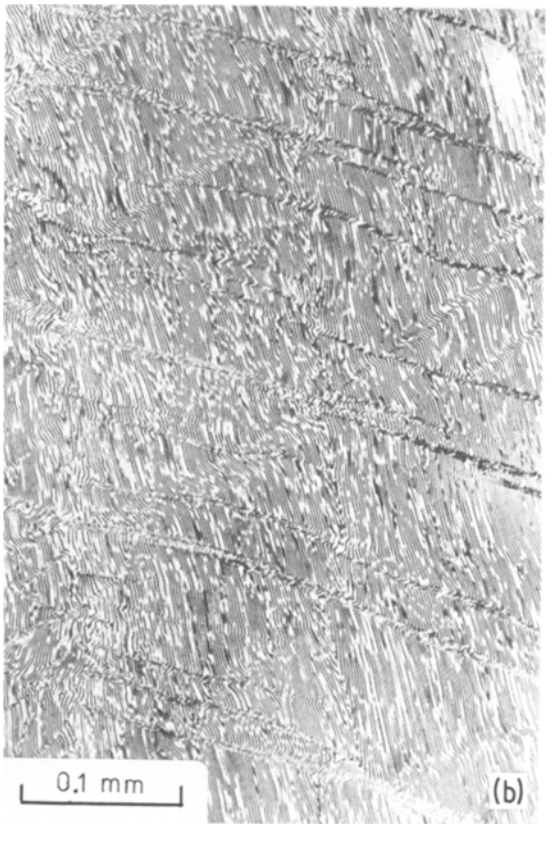

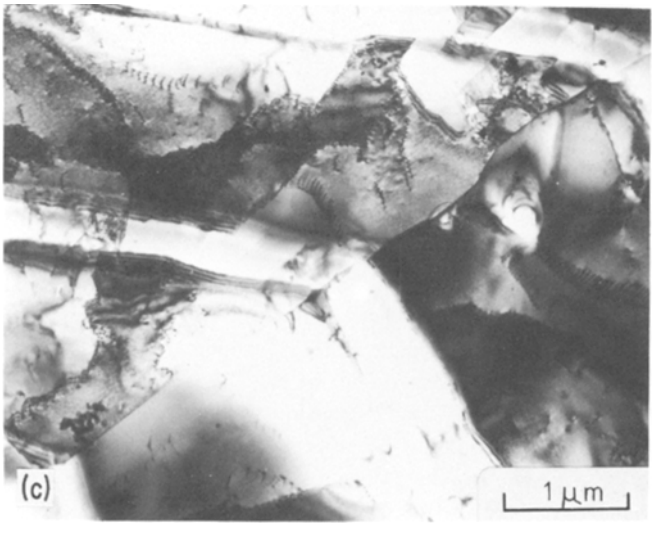

Figure 9 The effect of quenching on deformation of specimen C3; (a) photomacrograph of the deformed specimen showing the relatively even distribution of deformation bands. (b) optical micrograph showing the narrow width of the bands. (c) electron micrograph showing the large number of low-angle dislocation walls adjacent to the boundary of a deformation band.

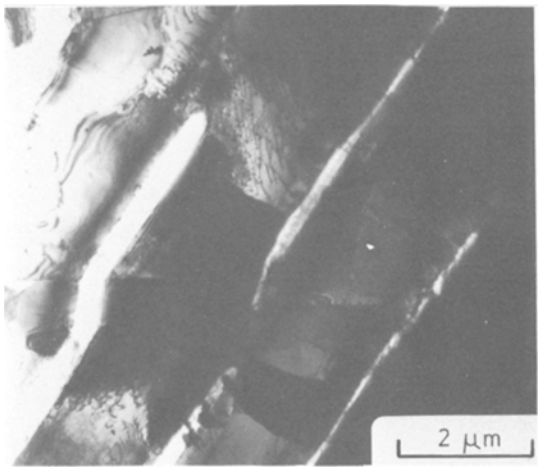

Figure 10 Electron micrograph showing the high density of dislocations at the tip of a kink band in specimen C2 (longitudinal section).

paring tensile and compressive deformation properties is more difficult for the Cd–Zn eutectic than for most other eutectic alloys because of the widely differing modes of deformation. However the fact that the alloy becomes stronger with quenching in both compression and tension implies that residual stresses are less important than the solution strengthening in the quenched material. This is understandable because room temperature is slightly greater than half the absolute melting temperature of the cadmium phase, hence recovery would be fairly rapid.

4.2.3. Geometric factors

Because the slip planes in each phase are parallel and both phases plastically at similar stress levels,

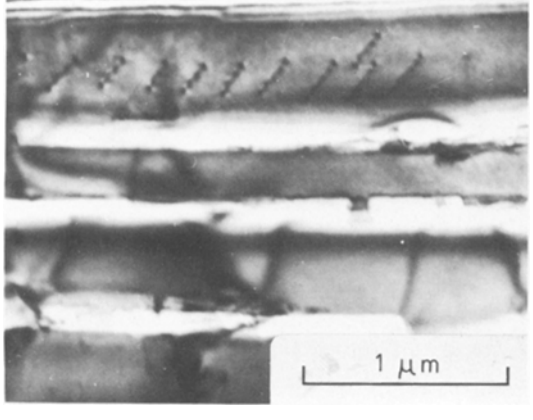

Figure 11 Electron micrograph showing a queue of basal dislocations in a Cd-rich lamella. Specimen E4; longitudinal section.

constraint caused by incompatiable plastic shear should not arise. However each phase having only one slip plane produces another possible source of constraint: the rotation of crystals due to basal glide. Geometrical softening [14], as it applies to single crystals, will not be significant since it is only important at relatively large plastic strains. However a complicating factor in the eutectic alloys is that adjacent grains may not have the same orientation and their respective rotations may oppose each other. This will produce lateral stresses constraining the deformation on the basal planes. The X-ray textures in Fig. 1 show that orientation variations about the growth axis increase with growth rate and it would therefore be expected that the constraints against rotation would also increase with decreasing λ.

All models incorporating geometrical constraint as a major factor in the strength fail on one point: their influence should increase with strain, rather than having most effect in the microstrain region.

4.2.4. Other possibilities

It can be seen from the arguments presented above that the commonly accepted explanations for the dependence of the strength of eutectic alloys on λ cannot be readily applied in the case of compressive deformation of the Cd–Zn eutectic. It is not only that kink formation is an unusual deformation mode but also because the deformation characteristics prior to kinking are atypical; evidence for the latter being that the yield stress is more sensitive to changes in λ than the strain-hardening rate. This is contrary to what is observed in other eutectic alloys (e.g. Al–Cu and Ag–Cu [15]). This implies that there may be a "friction stress" which is dependent on λ and, once this stress is exceeded, the increase in stress is a function only of the total shear strain. Speculation as to the cause of this behaviour might suggest that the imperfect interface structure is a source of long-range fluctuating stress, the amplitude of which decreases with increasing distance from the interface. If such a stress field could be shown then it could account for the compressive behaviour. However it conflicts with the results from the tensile tests [5] which show yield stress to be independent of λ. This might be because yield detected in tension is not due to basal glide but to some other process, such as expansion of twin nuclei. More experimental work would be necessary to clarify this.

A further possibility, for which no supporting experimental evidence is available, is suggested by the observation that the expected basal dislocation sources within the cadmium lamellae were not seen in as-quenched alloys under electron microscopy. Perhaps such sources need to be created during the microstrain region of deformation. A possible reaction which enables this to occur involves the intersection of two pyramidal dislocations. In the orientation of the eutectic phases there are two pyramidal systems which have equal Schmid factors: $(\bar{1}\bar{1}22)$, $[11\bar{2}3]$ and $(11\bar{2}2)$, $[11\bar{2}\bar{3}]$. These planes intersect in a $[1\bar{1}00]$ direction in the basal plane. For dislocations travelling from opposite sides of a lamella, the sum of Burger's vectors is $2/3[11\bar{2}0]$, which could yield two common $1/3[11\bar{2}0]$ types. Price [16] has suggested that pyramidal dislocations may split into partials with almost close-packed Burger's vectors of $1/6[20\bar{2}3]$. The reaction of the partials also leads to two $1/3$ $[11\bar{2}0]$ dislocations. The basal dislocations would be pinned to a large extent by the pyramidal sections connected to their source in the interface and could, therefore, presumably act as a source. The observed dependence of stress on λ during microstrain would then be expected, because the slip distance of the dislocations is determined by λ. Consequently, a higher stress would be required in the more finely spaced alloys to achieve the same density of basal dislocation sources. This also allows the relative insensitivity to λ of the linear strain hardening rate in compression when basal slip becomes dominant.

4.3. Coarsening during deformation

Accelerated coarsening of two-phase structures during hot-working is a well known phenomenon [17]. Once coarsening had commenced the aligned structure would have been lost, weakening that area and enabling deformation to proceed at a lower stress. Thus the stress elsewhere would have become too low to form new kinks and the deformation would have remained localized. In alloys with large λ, coarsening did not occur and the stress drop beyond σ_{max} was minimal. The transition in deformation microstructure from alloys with fine spacing to those with coarse spacing was gradual. Fig. 7 shows the slight coarsening within kink bands of an alloy with a moderate λ of 1.5 μm.

The preferential coarsening observed in the kink bands of the more finely spaced alloys can be seen as consistent with the commonly reported observation that low-angle grain boundaries promote coarsening of two-phase materials through enhanced diffusion and/or migration of the triple points [17, 18]. As well as the kink boundaries being very likely sites for coarsening, Fig. 8 shows that there were also low-angle boundaries within the kink and it is possible that these, too, could promote coarsening. The alloys with lower values of λ will, of course, have a higher amount of interfacial area per unit volume and therefore the driving force for coarsening will be greater in these.

Soutiere and Kerr [8] reported that there was accelerated coarsening within the kink bands when a coarsely spaced Cd–Zn eutectic alloy was deformed in compression and then annealed. This, they proposed, was due to the loss of preferred crystallography during deformation with consequent increase in interfacial energy. In fact, transmission electron microscopy in this study has revealed that the orientation relationship is maintained within kink bands. A more likely explanation for the accelerated coarsening is that the kink boundaries and the low angle boundaries within the kinks promoted coarsening in the same manner as discussed above for coarsening of the finely spaced eutectics during deformation.

5. Conclusions

A typical compressive stress–strain curve consists of an elastic portion, a linear strain-hardening region extending to a plastic strain of up to 0.01 followed by a stress peak and, for alloys with smaller interlamellar spacings, a subsequent rapid decrease in stress.

The yield stress (i.e. the stress at first detectable deviation from linearity) and the kinking stress increased with decreasing interlamellar spacing but the linear strain hardening rate was independent of spacing.

Kink bands formed at the stress peak in a manner which followed the model of Hess and Barrett and the localized increase in plastic strain led to a drop in stress. Well-formed kink band boundaries usually contained dislocations of more than one Burger's vector. Kink band formation occurred at a plastic strain which was independent of λ.

Electron microscopy provided strong evidence

for the operation of the basal slip system during compressive deformation. There was no evidence for pyramidal slip.

Coarsening of the more finely spaced alloys during deformation was promoted by the dislocation array which formed the kink boundary and by the low angle grain boundaries within the kink. They were probably also responsible for coarsening of kink bands with prolonged room temperature ageing.

References

1. B. J. SHAW, *Acta Met.* **15** (1967) 1169.
2. M. SAHOO, R. A. PORTER and R. W. SMITH, *J. Mater. Sci.* **11** (1976) 1680.
3. G. W. DELAMORE, R. H. VAN DE MERWE, M. SAHOO and R. W. SMITH, *ibid.* **16** (1981) 2313.
4. J. D. MEAKIN, *Can. J. Phys.* **45** (1967) 1121.
5. C. J. DAVIDSON and I. O. SMITH, *J. Mater. Sci.* **18** (1983).
6. M. BOOTH, M. GITTOS and P. WILKES, *Met. Trans.* **5** (1974) 775.
7. M. STRAUMANIS and N. BRAKSS, *Z. Phys. Chem.* **30B** (1935) 117.
8. B. SOUTIERE and H. W. KERR, *Trans. TMS-AIME* **245** (1969) 2595.
9. E. OROWAN, *Nature* **149** (1942) 643.
10. J. B. HESS and C. S. BARRETT, *Trans. TMS-AIME* **185** (1949) 599.
11. F. LASZLO, *J. Iron St. Inst.* **147** (1943) 173.
12. R. F. S. HEARMON, Landolt-Börnstein New Series, Vols. 1 and 2 (Springer-Verlag, Berlin, 1966, 1969).
13. Y. S. TOULOUKIAN, R. K. KIRBY, R. E. TAYLOR and P. D. DESAI, "Thermophysical Properties of Matter" (Plenum Press, New York, 1975).
14. R. W. K. HONEYCOMBE, "The Plastic Deformation of Metals" (Arnold, London, 1968) pp. 21–23.
15. C. J. DAVIDSON, PhD thesis, University of Queensland (1980).
16. P. B. PRICE, *Phil. Mag.* **5** (1960) 873.
17. J. J. JONAS, C. M. SELLARS and W. J. McG. TEGART, *Met. Rev.* **14** (1969) 1.
18. Y. G. NAKAGAWA and G. C. WEATHERLY, *Met. Trans.* **3** (1972) 3223.

Received 11 May
and accepted 31 August 1982